CIVIL ENGINEERING JOURNAL

Article no. 25

THE CIVIL ENGINEERING JOURNAL 3-2023

A NEW HYBRID FRAMEWORK OF MACHINE LEARNING TECHNIQUE IS USED TO MODEL THE COMPRESSIVE STRENGTH OF ULTRA-HIGH-PERFORMANCE CONCRETE

Xin Zuo[1], Die Liu[1], Yunrui Gao[1], FengJing Yang[2] and Gohui Wong[3]*

1. *Business School of Chongqing Institute of Humanities and Science and Technology, Chongqing, China*
2. *School of Architecture and Art, Chongqing Institute of Humanities and Technology, Chongqing, China*
3. *College of Civil Engineering, Architecture, and Environment, Wuhan, China, email: hbwh0314@163.com*

ABSTRACT

To calculate the compressive strength (CS) of concrete, it is necessary to investigate Ultra-High-Performance Concrete $(UHPC)$ in terms of its components and their quantities. Empirical analysis of relationships between constituents can be more time- and money-consuming. The CS can now be evaluated based on the composition of the ingredients thanks to intelligent systems. Additionally, it is advisable to promote the use of eco-friendly materials in concrete, one of the most commonly used materials in the world. The CS of $UHPC$ was attempted to model in this study. The CS of concrete has been simulated using Support Vector Regression (SVR), a Machine Learning (ML) technique that is compatible with Particle Swarm Optimisation (PSO) and Henry's Gas Solubility Optimisation $(HGSO)$, based on various materials used in the construction present article. The CS values were determined through the testing of eight components. The modeling process was evaluated using a variety of metrics. In this regard, the test phase modeling's root-mean-square error $(RMSE)$ for $SVR-HGSO$ was 8.45, while it was 9.23 for $SVR-PSO$. $SVR-HGSO's\ RMSE$ rate for the training phase was calculated at 10.15, which is 3.3 percent higher than $SVR-PSO's\ RMSE$ of 10.49.

KEYWORDS

Compressive strength, Support vector regression, Ultra-High-Performance Concrete, Particle swarm optimization, Henry's Gas Solubility Optimization

INTRODUCTION

Superior mechanisms and persistence capabilities, like self-compactness, in constructions, compressive strength (CS) of more than $150\ Mpa$, and exceptional durability in any challenging environments, use Ultra-High-Performance Concrete $(UHPC)$ as a suitable material [1]–[4]. Reducing the cement and micro-silica content significantly lowers costs and $CO2$ emissions, even despite the high initial cost and negative environmental impact, the practical qualities and extended service life compared to conventional or high-strength concrete are justifiable. Cement reduction, which is crucial in this regard, can boost the construction industry's sustainability by resulting in more environmentally friendly structures [5]. Numerous studies have recently examined $UHPC$ usage and behaviour [6], where $UHPC$ typically displays CS that range from $150\ MPa$ to $810\ MPa$ [7]–[9]. Researchers are interested in using materials like micro-silica, fly ash, metakaolin, and nano-silica in the design of concrete mixtures. Furthermore, since the assets are used to address various

aspects of the concrete and the design of the concretes is primarily based on CS, comparing their effects on the mechanical features of concrete has the greatest interest [10], [11].

The Portland cement-like fly ash helps produce concrete with less water by having a shape and size similar to Portland cement. Fly ash and superplasticizers are best blended to enhance the mechanical properties of concrete, particularly its CS. The cost, durability, workability, and water permeability of concrete, on the other hand, are all significantly impacted by the addition of fly ash. Fly ash is frequently used to replace sticky substances in construction projects. While highlighting the environmental advantages, using fly ash in concrete mixtures lowers the risk of contamination [12]–[14]. Fly ash can replace $20-50\%$ of the total adhesion of concrete and can even be increased to 60% if the initial strength of the concrete is a crucial factor [15], [16].

Concrete with a similar shape to pozzolan is mixed with a different amount of cement, changing how practical concrete behaves [17]–[20]. Because of the silica fumes' small particle size, it can serve as both a filler and a pozzolan in the concrete mixture [21]. The concrete's short-term $(28-day)$ CS would be improved despite the increasing proportion of silica fume inside the concrete that reduces the concrete's ability to be worked [22]. It is not always possible to determine with absolute certainty which silica fume will achieve the best CS. To increase the CS of concrete, researchers substitute various percentages of silica fume [23], [24]. Since the particles are smaller than those of cement, the silica vapour reaction improves the properties of concrete similarly to pozzolan [25]–[30]. Micro-silica with superplasticizers improves CS in the context of fly ash by lowering porosity [31].

The use of Machine Learning (ML) techniques in civil engineering is very widespread. Such solutions have the researchers' view for appraising concrete properties [32]–[35]. The $UHPC$ presence entails more progress in modeling with Artificial Intelligence (AI) for knowing the behavior of concrete overloading. Many methods to model the performance of $UHPC$ have been successfully introduced by experts in several studies [36]–[38]. These techniques depend on a dataset to create a trustworthy model, and the accuracy of their results depends on the species discovered through experimentation or the dataset drawn from the literature. One study included sugarcane bagasse ash and used a gene expression program to estimate the CS of concrete [39]. By contrasting the model's output with empirical strength measurements, the accuracy of the model was determined. In other research, a framework for evaluating the compressive strength of cement made of nano- and micro-silica was developed using genetic programming [40]. One study proposed a silica fume-based model for predicting the CS of concrete [41]. To lessen the expense and complexity of the developed model, they used Artificial Neural Networks (ANN) and had the grey wolf optimisation algorithm (GWO) algorithm optimise their model.

In the current study, a ML method based on the Support Vector Regression (SVR) method is investigated. This method makes use of the algorithms to predict the CS of concrete. In this regard, Particle Swarm Optimisation (PSO) and Henry's Gas Solubility Optimisation $(HGSO)$, two novel optimization algorithms, are used to more accurately model the CS of $UHPC$. R^2, VAF, OBJ, and MAE are four indices that are used to assess the modeling process; they are thoroughly introduced in Table 3.

From a paper on $UHPC$, CS studies, an experimental research dataset with numerous parameters is gathered [42]–[44]. Ingredients needed to produce high $UHPC$ is 1) fine powders (silica fume crushed, nano-silica, and quartzite), 2) lower water/binder ratio (below 0.2), 3) cement (more than 800 kg/m^3); 4) high range water-reducing admixture, and 5) steel fibers as well as polyethylene fibers [45].

Therefore, coupled frameworks of $SVR-PSO$ and $SVR-HGSO$ attempt to feed on data of ingredients of concrete and target values of CS and then generate the $UHPC$ persistence rates with various ingredients. The specific information needed for modeling is displayed in the following section.

MATERIALS AND METHODOLOGY

The clear methods provided in this sector are required for the probe of models that attempt to the results of ingredient compositions should be estimated in terms of CS for $UHPC$. Two potent optimization algorithms work in tandem with the capable SVR to avoid estimating the necessary parameters while locating the best modeling framework. To improve the accuracy of simulating the CS of various sample compositions, the $SVR-PSO$ and $SVR-HGSO$ have been developed. For samples, the data published in [42]–[44] are available. Table 1 provides a brief overview of the information gathered from 110 experimental samples in this regard. The various CSs of each sample are produced by combining the aforementioned ingredients in different amounts.

Simulating their resistance is modeled with the mathematical solutions elaborated on in this section. Also, Fig. 1 exhibits the CS derived from the various mixtures of items presented in Table 1, in which each colorful string represents one sample out of 110 samples.

Tab.1 - Input and target data for predictive models

Ingredient	$Unit$	$Symbol$	Statistical measurements				
			Min	Max	$Mean$	$Median$	$St.dev$
$Cement$	(kg/m^3)	CE	383	1600	879.7	786	329.8
$Silica\ fume$	(kg/m^3)	SI	30	367.95	192	196	94.6
$Fly\ ash$	(kg/m^3)	FA	120	448	33	120	72.7
$Sand$	(kg/m^3)	SA	292	1898	980	1107	513.8
$Steel\ fiber$	(kg/m^3)	SF	2	470	39	8	74.8
$Quartz\ powder$	(kg/m^3)	QP	203.3	750	36.9	211	125.9
$Water$	(kg/m^3)	WA	109	334.5	197.1	185.3	54.3
$Admixture$	(kg/m^3)	AD	4	185	31.9	30.1	28.2
$Compressive\ strength$	(MPa)	CS	95	240	152.2	147.9	31.5

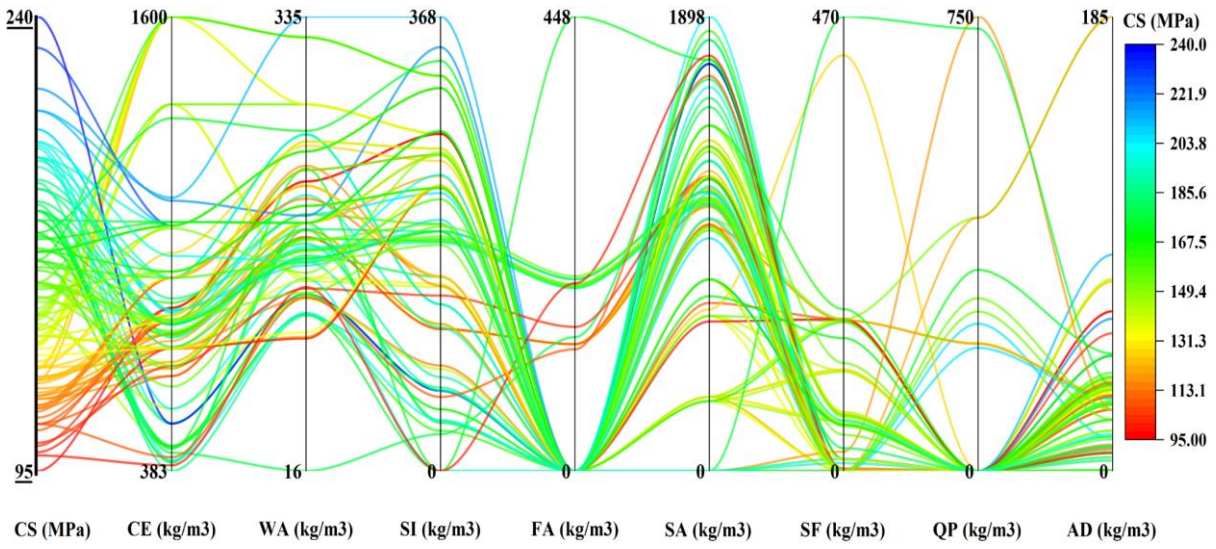

Fig. 1 – The compressive strength of various mixtures of ingredients

Henry's gas solubility optimization algorithm, $HGSO$

Henry's Law of Physics is used to construct the $HGSO$ [46]. The aforementioned regulation was developed by the maximum amount of dissolved solute envisioned at a specific pressure and temperature level [47]. Applying the aforementioned rule makes it possible to demonstrate the

solubility of low-soluble gases in the unique solvent. The ability of solubility has been largely influenced by temperature and pressure; for gases, the pressure parameter is reduced by increasing the temperature variable, and the relationship is appropriate for solids. Pressure's incremental trend contributes to an increase in solubility [48]. The gas and the pertinent solubility were used in the study by Hashemian et al. to develop the Henry law [46]. The following lists the steps needed for $HGSO$:

1- Establishing the precise location and quantity of gases (creating the initial population).

2- Creating population classes based on gas type characteristics.

3- figuring out the cost of the classes, selecting them, and selecting the ones with the best results to assign appropriate conditions.

4- Updating the coefficients of Henry's law.

$$H_j(t+1) = H_j(t) \times e^{\left(-C_j\left(\frac{T^\theta - T(t)}{T(t)\times T^\theta}\right)\right)} \quad (1)$$

$$T(t) = e^{\left(\frac{t}{iter}\right)} \quad (2)$$

In which the H_j shows the Henry law coefficient for class j .C_j and T^θ Alternatively, exhibit a random and constant number of $[0\ to\ 1]$. Also, the variables of $iter$ and t represent, respectively, the number of iterations in the queue and temperature.

5- Update of the factor of solubility using Eq. (3).

$$S_{i,j}(t) = K \times H_j(t+1) \times P_{i,j}(t) \quad (3)$$

where K displays a constant value; $P_{i,j}(t)$ and $S_{i,j}$ represent the solubility and pressure of gas i^{th} in the class of j, alternatively.

6- Next, the location of the primitive population is updated using Eq.s $(4, 5)$.

$$X_{i,j}(t+1) = X_{i,j}(t) + F \times r \times \gamma \times \left(X_{i,best}(t) - X_{i,j}(t)\right) + F \times r \times \alpha \times \left(P_{i,j}(t) \times X_{best}(t) - X_{i,j}(t)\right) \quad (4)$$

$$\gamma = \beta \times e^{\left(-\frac{F_{best}(t)+\varepsilon}{F_{i,j}(t)+\varepsilon}\right)} + \varepsilon \quad (5)$$

In which $X_{i,j}$ describes where the gas of i in the class of j. Variables of $F_{i,j}$ and F_{best} demonstrates the population in cluster j and the best cost of petrol i. Parameters of $X_{i,best}$ and X_{best} indicate, instead, the preferred gas in the class of j and the population. Additionally, the r parameter displays a random number between $[0\ and\ 1]$. α and β , as a fixed number, are determined 1 as well as ε, which is 0.05. γ additionally displays the probable interaction between the gases.

7- To satisfy the regional minimum trapping standards, the worst petrol number is assigned.

$$N_w = N \times (rand(C_2 - C_1) + C_1) \quad (6)$$

In which, C_1 and C_2 are fixed, as 0.1 and 0.2, alternatively, and the N shows the population.

8- The worst gas location can be calculated with Eq. (7).

$$G_{i,j} = G_{Min(i,j)} + r \times \left(G_{Max(i,j)} - G_{Min(i,j)}\right) \quad (7)$$

In which G_{Min} and G_{Max} are, respectively, the lower and upper boundaries. The variable of $G_{i,j}$ denotes the gas i location in the class of j.

Particle swarm optimization algorithm, PSO

Known as a population-based solution, the PSO algorithm. PSO was created with an eye toward the feedback of animal group interactions. Essentially, this approach was proposed in a study that $Kennedy\ et\ al.$ [49], who elaborated it extensively [50]–[53]. This makes the location and the velocity parameter essential components of population control. The first of two scoring schemes is taken into consideration, and the best global position is the one that best fits the placement of the particles. To reach the maximum number of iterations, particle location, and velocity are determined iteratively. Updates to the locations and velocities are made by the equations below.

$$P.v_{ij}^{new} = WP.v_{ij}^{current} + C_1 r_1 (P.p.best_{ij}^{new} - P.p_{ij}^{current}) + C_2 r_2 (Global.best_{ij}^{current} - P.p_{ij}^{current}) \quad (8)$$

$$P.p_{ij}^{new} = P.p_{ij}^{current} + P.v_{ij}^{new} \quad (9)$$

where W stands for the inertia factor. $P._v$ and $P._p$ display the position and speed of the particles. The accidental number of $(0\ to\ 1)$ is represented by the variables r_1 and r_2. C_1 and C_2 are used to calculate the acceleration factors for local and global learning, respectively. The best solutions from all swarms are represented by the Global best variable.

Support Vector Regression, SVR

SVR, was introduced to classify regression problems [54]. Support vector machine (SVM) regression refers to a SVR machine that uses a tolerance region (ε) to determine a regression. In the SVR approach, regression class classification is utilized to design a hyperplane optimized. To find answers to questions about regression and to create the following features, SVR was combined with supervised learning techniques [55]:

$$min_{w,b} = \frac{1}{2}\|w\|^2 + C\sum_{i=1}^{m}(\xi_i + \xi_i^*) \quad (10)$$

$$s.t. \quad \begin{Bmatrix} y_i - (w^T x_i + b) \le \varepsilon + \xi_i \\ (w^T x_i + b) - y_i \le \varepsilon + \xi_i^* \\ \xi_i, \xi_i^* \ge 0 \end{Bmatrix}$$

The specifications of w, C, b, ξ, and ε, alternately represent the bias, amount of boundary exceeding, coefficient weight, queue regularisation factor, and rate of deviation from the hyper-plane. Two concepts are included in the function of fitness:

$$\frac{1}{2}\|w\|^2 \quad (11)$$

$$C\sum_{i=1}^{m}(\xi_i + \xi_i^*) \quad (12)$$

Equation (11) was used to maintain the distance between the sample and the hyperplane while modifying Equation (12) to widen the gap between the sample and the hyperplane. When creating a function with a hyperplane target, appropriate values of b and w were gathered. To achieve the desired outcome for this study, a quadratic objective function was used [56]. The main responsibility of the SVR has been to determine the defining parameters in the optimal levels (ε, $sigma$, and C) that are indicated in Table 2.

Tab. 2 – The determining variables' magnitudes of each optimizer

		$SVR-HGSO$	$SVR-PSO$
Training phase	C	3.050	0.05
	$EPSILON$	139.302	1298.62
	$GAMA$	0.066	0.05
Testing Phase	C	0.301	3.781
	$EPSILON$	28.094	2981
	$GAMA$	0.070	2

SVR was combined with a variety of optimizers, including $HGSO$ and PSO, to estimate parameters at the best level to locate pertinent parameters.

Criteria for evaluation of developed $SVR-HGSO$ and $SVR-PSO$

The various evaluators for measuring the CS of concrete samples using predictive frameworks are defined in Table 3.

Tab. 3 – The metrics used to evaluate models

$Indexes$	$Codes$	$Relations$	$Status$
Variance account factor	VAF	$\left(1-\frac{var(t_n-y_n)}{var(t_n)}\right)*100$	A high value means desirable
Mean absolute error	MAE	$\frac{1}{N}\sum_{n=1}^{N}\lvert p_n-t_n\rvert$	A low value means desirable.
Root mean squared error	$RMSE$	$\sqrt{\frac{1}{N}\sum_{n=1}^{N}(p_n-t_n)^2}$	$A\ low\ value\ means\ desirable.$
Pearson's correlation coefficient	R^2	$\left(\frac{\sum_{n=1}^{N}(t_n-\bar{t})(p_n-\bar{p})}{\sqrt{[\sum_{n=1}^{N}(t_n-\bar{p})^2][\sum_{n=1}^{N}(p_n-\bar{p})^2]}}\right)^2$	$A\ high\ value\ means\ desirable$
Statistical parameters, including the various error indices	OBJ	$\left(\frac{n_{train}-n_{test}}{n_{train}+n_{test}}\right)\frac{RMSE_{train}+MAE_{test}}{R^2_{train}+1}+\left(\frac{2n_{train}}{n_{train}+n_{test}}\right)\frac{RMSE_{test}-MAE_{test}}{R^2_{test}+1}$	A low value means desirable [57]

In mentioned relations, p_N exhibits the magnitude of predicted CS; t_n is the n^{th} target value (as measured); $\bar{t}$ is the measured data as calculated averagely; $\bar{p}$ represent the averaged target values of CS and the variables for the phases of training and testing, respectively, the n_{train} and n_{test} which are the collected number of CS relevant steps of train or testing.

RESULTS AND DISCUSSIONS

The results of modeling $UHPC$ in 110 compound samples were produced using both frameworks. In addition, to better understand the capabilities of each proposed model, the performance evaluation indices evaluated the $SVR-HGSO$ and $SVR-PSO$ modeling processes. In the initial step, the simulated results of each sample's CS are shown in front of the actual numbers. In this regard, Fig. 2 displays the CSs that S$VR-HGSO$ modeled.

The aforementioned optimization algorithms and the SVR model are created independently in the Matlab software before being combined to create the hybrid framework. The optimization algorithm is viewed as the primary function in the modeling process, and the SVR model is taken to be the cost function. The optimization algorithm defines the input variables, target variables, and the hey parameter of SVR in each step, and the SVR model provides predictions corresponding to these variables. The maximum iteration serves as the stopping criterion, and the $RMSE$ value is used to determine which model is best developed. Additionally, Appendix A now includes a brief program of the $SVR - PSO$ model development.

Tab. 4 - Comparison of present study results with recently published articles with similar datasets.

$Work\ ID$	$Model$	R^2
Wu [1]	$FDA - RBF$	0.916
$R.Abuodeh\ et\ al.$ [2]	$BPFNN$	0.8
$Alabduljabbar\ et\ al$ [3]	$Gene\ expression$	0.969
$Present\ Work$	$SVR - HGSO$	0.964

A comparison of the present study with published articles that studied similar fields is presented in Table 4. This table is presented as an identifier of the developed hybrid model performance and workability compared to recent studies. The results obtained from the $SVR - HGSO$ show its higher capability in predicting the CS of $UHPC$.

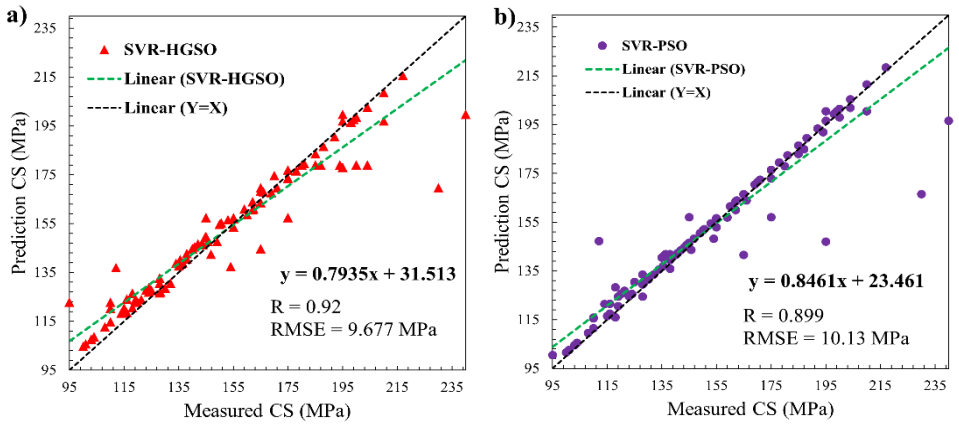

Fig. 2 – Estimated CS by: a) $SVR - HGSO$ and b) $SVR - PSO$

As seen in Figure 2, the results of each model are at an acceptable rate. $SVR - HGSO$ was able to model the CS variables 2.31 percent better than $SVR - PSO$ due to its higher R^2 at the level 0.92. Similar to this, the other model performed this task better, with a 4.69 percent lower $RMSE$ index, and was able to model the compounds' CS factor with a 10.13 MPa error. The slope of the trendline for the PSO-owned model, however, could be found to be better with a value of 0.84, this is 6.33 percent higher than SVR-HGSO, indicating that certain points between the samples with numbers 195 to 210 that are outside the best-fit line may have been the source of this event.

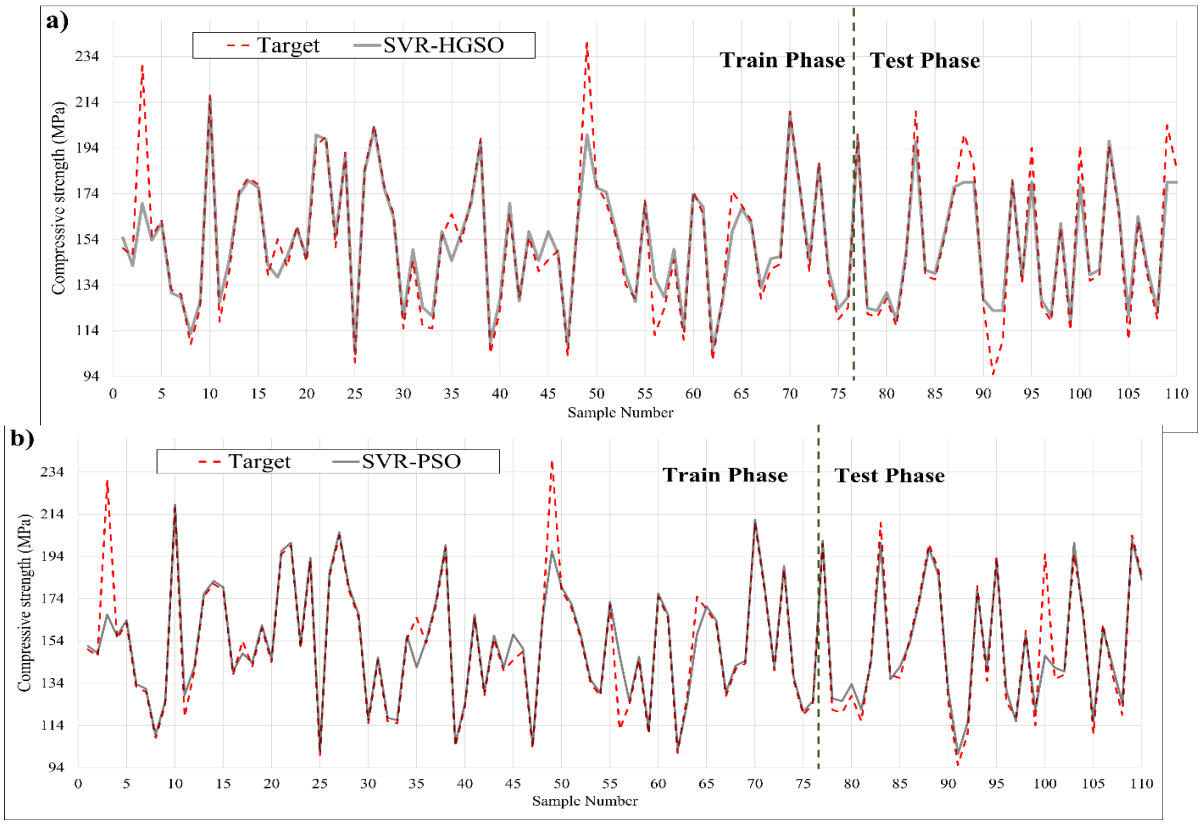

Fig. 3 –Estimated and Target values CS appraised by: a) $SVR-HGSO$ and b) $SVR-PSO$

Surveying Figure 3, the training stages are approximately identical to each other except for some parts, such as samples with the numbers 32 and 33, which are modeled more accurately by the $SVR-PSO$ with errors of 1.31% and 1.32%, respectively, while by the $SVR-HGSO$ the errors are 7% and 4.7%. With an error of 1.28 percent in $SVR-PSO$ versus 3.96 percent in $HGSO$, the sample of 75 also produced better modeling results. In the testing phase, $PSO's$ grey lines could be used to demonstrate that, when compared to $SVR-HGSO$, $SVR-PSO's$ grey lines are more closely aligned with the target red dashed lines. $SVR-HGSO$, on the other hand, better models the sample size of 100 with an error of 8.70%, whereas $SVR-PSO$ models this sample with an underestimation error of 24.61%. In order to better comprehend the disagreement in modelling CS values, Figure 4 makes an attempt to illustrate the variations in CS magnitudes between the two proposed models.

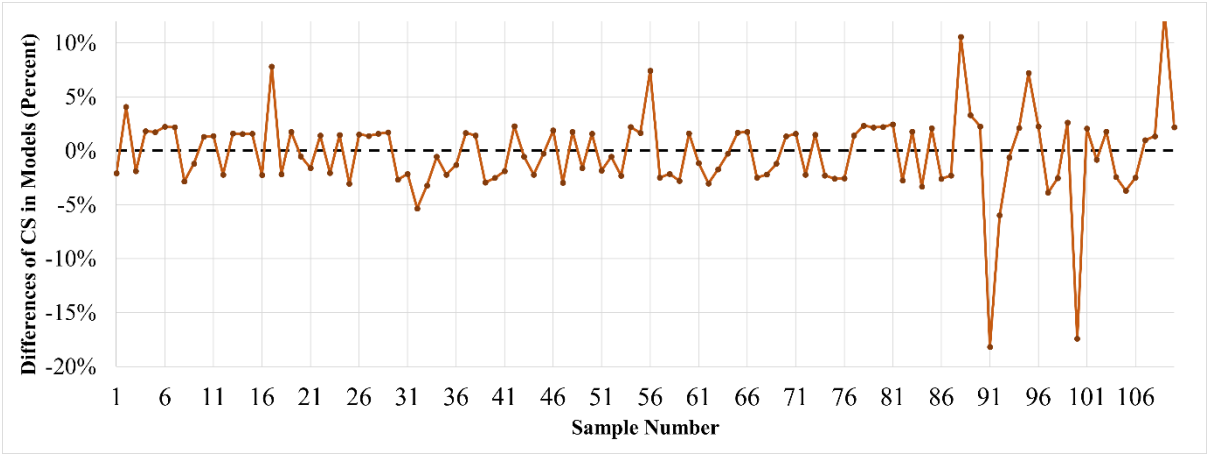

Fig. 4 – Difference between estimated CSs and developed frameworks.

It is noteworthy that Figure 4 was produced in the first stage by dividing the CS values modeled from $SVR-PSO$ by $SVR-HGSO$. Overall, the majority of the samples (samples 1 to 77) are modeled similarly, with a difference of 5% in the training phase. However, some examples in the testing phase, like 17, 32, and 56 samples, could be simulated with more than a five percent difference. On the other hand, samples $88, 91, 95, 100$, and 109 were modeled with different rates for the testing phase.

Figure 5 attempts to indicate the errors involved in modeling the CS of samples at the next stage. Any deviations from the measured $CS's$ target value lead to a gap from the zero line. Based on Figure 5 (a), the capability of $SVR-HGSO$ to model In contrast to $SVR-PSO$, the compressive resistance of samples is modeled with high-rate fluctuations. In place of $SVR-HGSO$, the smoother error line can be seen in the Training section. Every single point in the highlighted area is incorrect that are between -15% and $+23\%$ lower than $SVR-PSO$, despite the third sample of $SVR-HGSO$ having more errors of 27% during the training phase.

Additionally, the $SVR-HGSO$ 0-line does not have as many points as the $SVR-PSO$ 0-line that are touched by the evaluation indices. The $SVR-HGSO$ model includes a large number of samples for the testing phase. In contrast to $SVR-PSO$, which gave the Testing section a smoother line around the 0 error line, they are far from the 0 error line. The $SVR-HGSO$ in the sample of 91 exhibits the highest error rate in Figure 4, with a 29.28 percent error. The outcomes of the model's performance should be examined, as was already mentioned. Four assessment criteria that were used in the current study to evaluate models are shown in Figure 5.

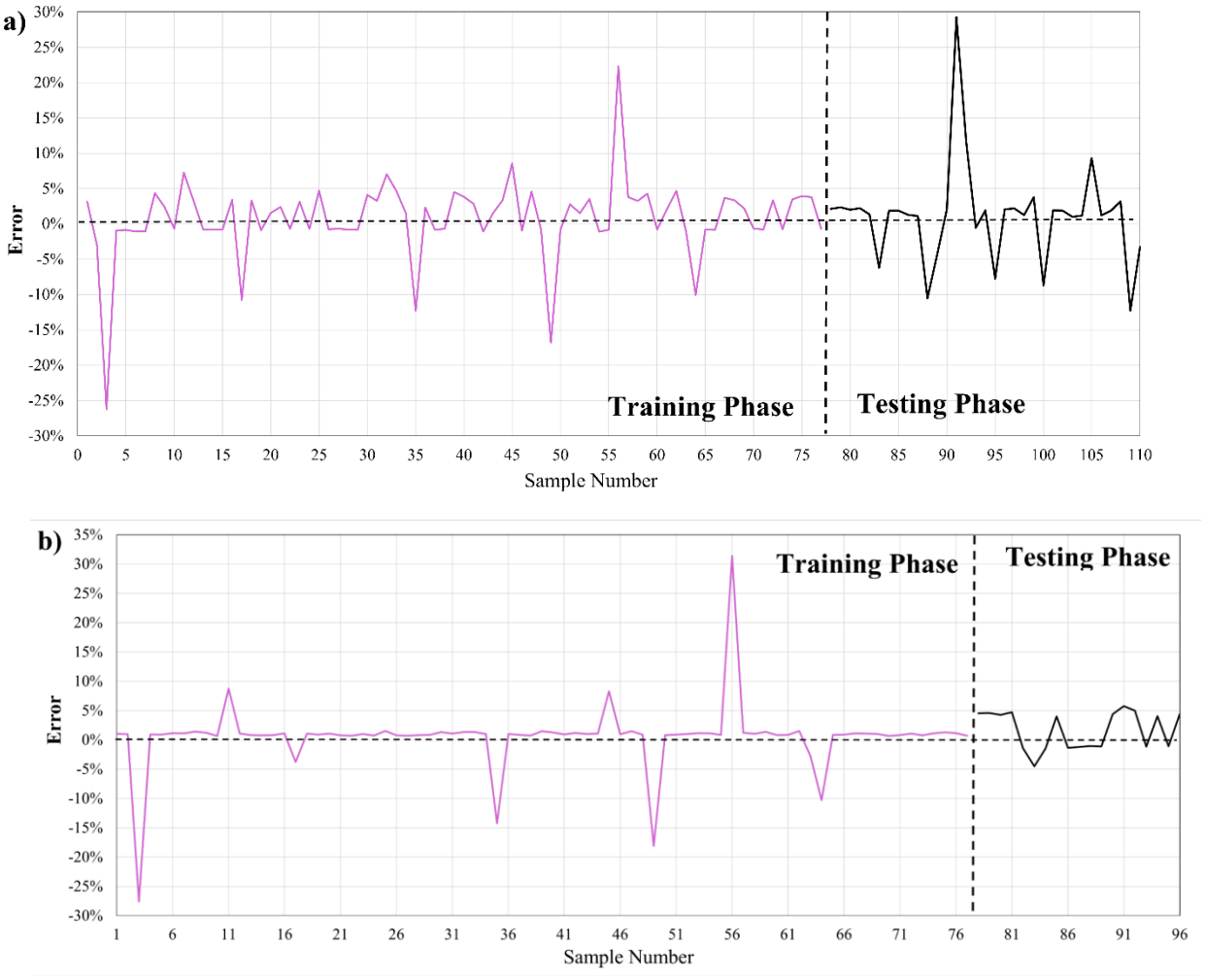

Fig. 5 – Error rates of CS modeling by a) $SVR-HGSO$ and b) $SVR-PSO$

$SVR-HGSO$ has demonstrated improved performance for the three statuses of training, testing, and total in the index R^2 for models. With a value of 0.96, the testing phase has a higher R^2 value, which is 3.84% higher than $SVR-PSO$. $SVR-PSO$ in the Training section could achieve the worst circumstance for the $RMSE$ error index with a value of $10.492\ MPa$, which is 3.33 percent higher than the rest. However, during the Testing section, $SVR-HGSO$ could only obtain $8.451\ MPa$ while $SVR-PSO$ obtained $9.23\ MPa$; this represents a 9.25% difference between the two models' simulations of the CS values under better conditions contrast to the $RMSE$ indicator, the $SVR-HGSO's$ performance from the MAE viewpoint from the $SVR-PSO's$ according to Fig. 6, performance for three conditions is ranked higher from an MAE perspective. $SVR-HGSO's$ testing phase had a CS calculation error of $5.644\ MPa$, which is 20% more than $SVR-PSO's$. The VAF criterion also demonstrated how closely the outcomes of the two models matched one another. With a difference of 2.22% for both the training and testing phases, the $SVR-HGSO$ could outperform the $SVR-PSO$ when the entire data set is taken into account. With rates of 92.21 and 96.33, the differences are roughly two percent in favour of $SVR-HGSO$. Except for the VAF index, $SVR-HGSO$, and $SVR-PSO$, the OBJ indicator that encompasses all of the criteria mentioned in both phases obtained magnitudes of 7.575 and 6.747, indicating the $SVR-HGSO's$ superior performance with a 12.27% advantage over other models.

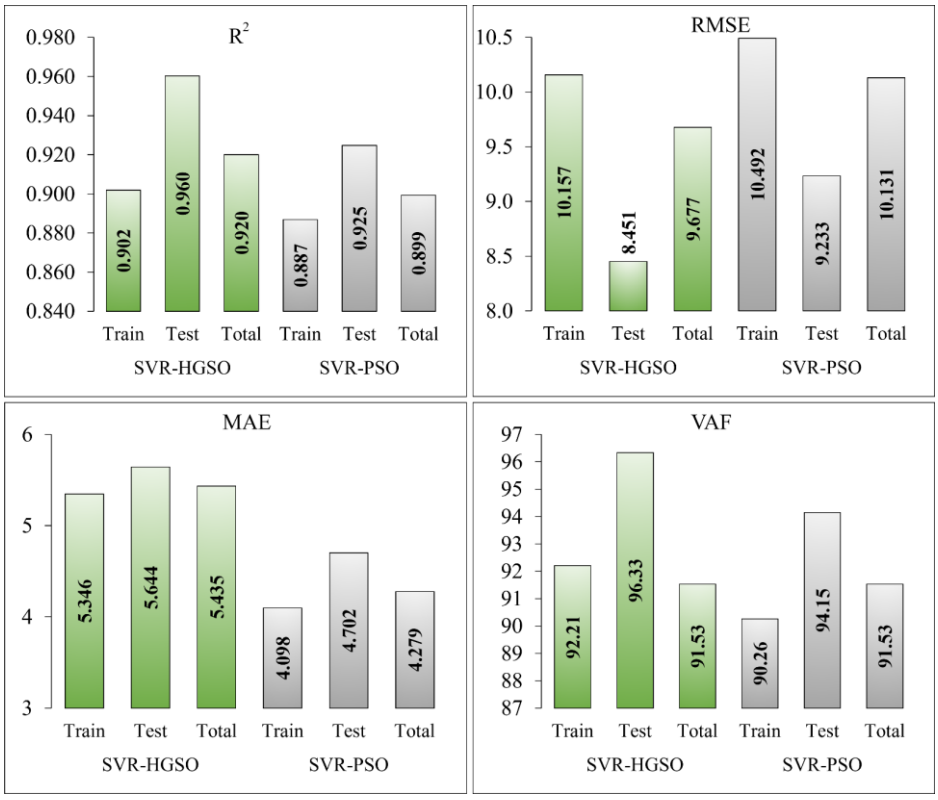

Fig. 6 – Evaluation indices' results for the performance of the proposed model

In the next stage, the distribution of errors for both models has been shown through Figure 7 that for $SVR-HGSO$, the errors are non-regularly spread over the horizontal axis with low concentrations around the 0 point of error. However, for $SVR-PSO$, this condition seems better with a suitable distribution of errors around 0 error. The bell-shaped normal distribution curves of error also show the thinner $SVR-PSO$ in front of the flatter $SVR-HGSO$ curve.

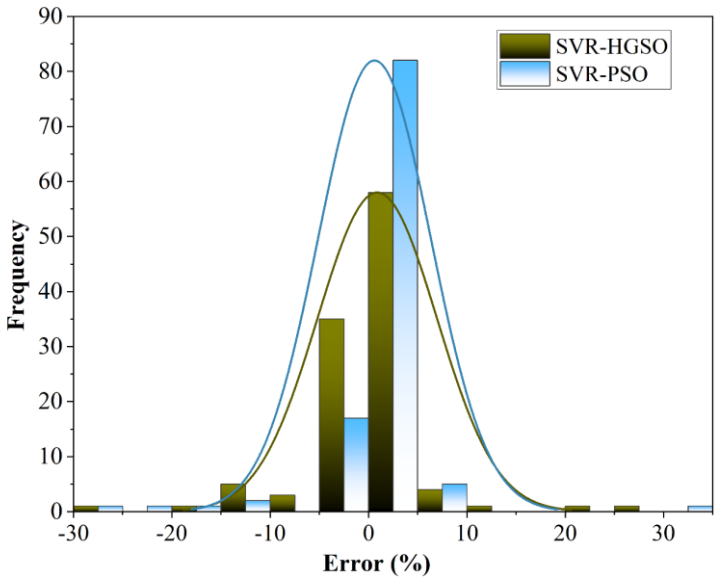

Fig. 7 – Error distribution of CS modeled via developed $SVR-HGSO$ and $SVR-PSO$

CONCLUSION

Ultra-high-performance concrete $(UHPC)$ is a widely used substance that produces buildings with exceptional performance, capabilities, and remarkable durability in any challenging environment. Reducing the cement and micro-silica content significantly lowers costs and $CO2$ emissions, even though the useful qualities and extended service life in comparison to regular or high-strength concrete compensate the pricey initial investment and negative environmental effects. Numerous studies have looked at the behavior of $UHPC$, which typically exhibits a CS of between $150\ MPa$ and $810\ MPa$. In some recent studies, various models were used to predict the CS of $UHPC$ concrete. Regarding these studies, it made sense that there wasn't a hybrid automated framework of predictive models. Consequently, a novel hybrid framework was created in the current study, and the presented models made a significant contribution is defined as follows:

- The SVR method, which employed the algorithms to predict concrete CS, was examined as a ML technique.
- $SVR-HGSO$ and $SVR-PSO$, two novel optimization algorithms, are used to more accurately model the CS of $UHPC$.
- With a difference of 2.31 percent, the $SVR-HGSO$ framework was able to model the CSs more accurately than $SVR-PSO$ thanks to its higher R^2 at the level of 0.92. $SVR-PSO$ was able to model the compounds' CS factor using the $10.13\ MPa$ error for the $RMSE$ index. While the other model performed this task more effectively than $SVR-HGSO$, with an $RMSE$ of 4.69 percent lower.
- Both models accurately predicted the CS values in the testing phase compared to the training phase. The $RMSE$ for $SVR-HGSO$ was $8.451\ MPa$, while the $RMSE$ for $SVR-PSO$ was $9.23\ MPa$, a difference of 9.25%.
- The VAF criterion also demonstrated how closely the outcomes of the two models matched one another. With a difference of 2.22% for VAF in both the training and testing phases, the $SVR-HGSO$ could outperform the $SVR-PSO$. The rates were 92.21 and 96.33, with differences of about 2% in favour of $SVR-HGSO$. The VAF index, the $SVR-HGSO$, and all of the other parameters specified in both phases were not included in the OBJ indication and the $SVR-PSO$, respectively, obtained values of 7.575 and 6.747, indicating that the $SVR-HGSO$ performed 12.27% better than the $SVR-PSO$.

- On the other hand, it is obvious that the search process of the $HGSO$ model in the exploration and exploitation outperformed compared to the PSO model, and delaying in local minimal for $HGSO$ is less than the PSO model.

To sum up, the $SVR - HGSO$ managed the error rates better than the $SVR - PSO$ visible in Figure 6 despite the accepted level of accuracy in modeling for both developed frameworks.

REFERENCES

[1] B. A. Graybeal, "Compressive behavior of ultra-high-performance fiber-reinforced concrete," *ACI materials journal*, vol. 104, no. 2, p. 146, 2007.
[2] P. Richard and M. Cheyrezy, "Composition of reactive powder concretes," *Cement and concrete research*, vol. 25, no. 7, pp. 1501–1511, 1995.
[3] Y. L. Voo and S. J. Foster, "Characteristics of ultra-high performance 'ductile'concrete and its impact on sustainable construction," *The IES Journal Part A: Civil & Structural Engineering*, vol. 3, no. 3, pp. 168–187, 2010.
[4] P. C. AITCIN, "Arts e scienza del calcestruzzo ad alte prestazioni," *L'Industria italiana del cemento*, vol. 68, no. 731, pp. 350–365, 1998.
[5] F. P. Torgal and S. Jalali, "Cement composites reinforced with vegetable fibres," in *Eco-efficient Construction and Building Materials*, Springer, 2011, pp. 143–156.
[6] C. Shi, Z. Wu, J. Xiao, D. Wang, Z. Huang, and Z. Fang, "A review on ultra high performance concrete: Part I. Raw materials and mixture design," *Construction and Building Materials*, vol. 101, pp. 741–751, 2015.
[7] Z. Yunsheng, S. Wei, L. Sifeng, J. Chujie, and L. Jianzhong, "Preparation of C200 green reactive powder concrete and its static–dynamic behaviors," *Cement and Concrete Composites*, vol. 30, no. 9, pp. 831–838, 2008.
[8] W. Zheng, B. Luo, and Y. Wang, "Compressive and tensile properties of reactive powder concrete with steel fibres at elevated temperatures," *Construction and Building Materials*, vol. 41, pp. 844–851, 2013.
[9] A. A. Pishro and X. Feng, "Experimental Study on Bond Stress between Ultra High Performance Concrete and Steel Reinforcement," *Civil Engineering Journal*, vol. 3, no. 12, pp. 1235–1246, 2018.
[10] Y. K. Cho, S. H. Jung, and Y. C. Choi, "Effects of chemical composition of fly ash on compressive strength of fly ash cement mortar," *Construction and Building Materials*, vol. 204, pp. 255–264, Apr. 2019, doi: 10.1016/j.conbuildmat.2019.01.208.
[11] M. Lezgy-Nazargah, S. A. Emamian, E. Aghasizadeh, and M. Khani, "Predicting the mechanical properties of ordinary concrete and nano-silica concrete using micromechanical methods," *Sādhanā*, vol. 43, no. 12, p. 196, Dec. 2018, doi: 10.1007/s12046-018-0965-0.
[12] J.-S. Chou and A.-D. Pham, "Smart Artificial Firefly Colony Algorithm-Based Support Vector Regression for Enhanced Forecasting in Civil Engineering," *Computer-Aided Civil and Infrastructure Engineering*, vol. 30, no. 9, pp. 715–732, Sep. 2015, doi: 10.1111/mice.12121.
[13] M. H. Rafiei, W. H. Khushefati, R. Demirboga, and H. Adeli, "Supervised Deep Restricted Boltzmann Machine for Estimation of Concrete.," *ACI Materials Journal*, vol. 114, no. 2, 2017.
[14] M. Castelli, L. Trujillo, I. Goncalves, and A. Popovic, "An evolutionary system for the prediction of high performance concrete strength based on semantic genetic programming," *Computers and Concrete*, vol. 19, no. 6, pp. 651–658, 2017.
[15] L. Lam, Y. L. Wong, and C. S. Poon, "Effect of Fly Ash and Silica Fume on Compressive and Fracture Behaviors of Concrete," *Cement and Concrete Research*, vol. 28, no. 2, pp. 271–283, Feb. 1998, doi: 10.1016/S0008-8846(97)00269-X.
[16] K. Ganesh Babu and G. Siva Nageswara Rao, "Early strength behaviour of fly ash concretes," *Cement and Concrete Research*, vol. 24, no. 2, pp. 277–284, 1994, doi: 10.1016/0008-8846(94)90053-1.
[17] L. G. Li, J. Zhu, Z. H. Huang, A. K. H. Kwan, and L. J. Li, "Combined effects of micro-silica and nano-silica on durability of mortar," *Construction and Building Materials*, vol. 157, pp. 337–347, Dec. 2017, doi: 10.1016/j.conbuildmat.2017.09.105.
[18] H. Eskandari, A. M. Nic, and A. Ghanei, "Effect of Air Entraining Admixture on Corrosion of Reinforced Concrete," *Procedia Engineering*, vol. 150, pp. 2178–2184, 2016, doi: 10.1016/j.proeng.2016.07.261.
[19] Z. Zhang, B. Zhang, and P. Yan, "Comparative study of effect of raw and densified silica fume in the paste, mortar and concrete," *Construction and Building Materials*, vol. 105, pp. 82–93, Feb. 2016, doi: 10.1016/j.conbuildmat.2015.12.045.
[20] A. Madadi, H. Eskandari-Naddaf, and M. Gharouni-Nik, "Lightweight Ferrocement Matrix Compressive Behavior: Experiments Versus Finite Element Analysis," *Arabian Journal for Science and Engineering*, vol. 42, no. 9, pp. 4001–4013, Sep. 2017, doi: 10.1007/s13369-017-2557-4.

[21] B. B. Sabir, “Mechanical properties and frost resistance of silica fume concrete,” *Cement and Concrete Composites*, vol. 19, no. 4, pp. 285–294, Jan. 1997, doi: 10.1016/S0958-9465(97)00020-6.
[22] M. Mazloom, A. A. Ramezanianpour, and J. J. Brooks, “Effect of silica fume on mechanical properties of high-strength concrete,” *Cement and Concrete Composites*, vol. 26, no. 4, pp. 347–357, May 2004, doi: 10.1016/S0958-9465(03)00017-9.
[23] S. Bhanja and B. Sengupta, “Influence of silica fume on the tensile strength of concrete,” *Cement and Concrete Research*, vol. 35, no. 4, pp. 743–747, Apr. 2005, doi: 10.1016/j.cemconres.2004.05.024.
[24] M. Y. Mansour, M. Dicleli, J. Y. Lee, and J. Zhang, “Predicting the shear strength of reinforced concrete beams using artificial neural networks,” *Engineering Structures*, vol. 26, no. 6, pp. 781–799, May 2004, doi: 10.1016/j.engstruct.2004.01.011.
[25] Z. Bajja, W. Dridi, A. Darquennes, R. Bennacer, P. Le Bescop, and M. Rahim, “Influence of slurried silica fume on microstructure and tritiated water diffusivity of cement pastes,” *Construction and Building Materials*, vol. 132, pp. 85–93, Feb. 2017, doi: 10.1016/j.conbuildmat.2016.11.097.
[26] M. Rostami and K. Behfarnia, “The effect of silica fume on durability of alkali activated slag concrete,” *Construction and Building Materials*, vol. 134, pp. 262–268, Mar. 2017, doi: 10.1016/j.conbuildmat.2016.12.072.
[27] H. Li, H. Xiao, J. Yuan, and J. Ou, “Microstructure of cement mortar with nano-particles,” *Composites Part B: Engineering*, vol. 35, no. 2, pp. 185–189, Mar. 2004, doi: 10.1016/S1359-8368(03)00052-0.
[28] L. P. Singh, S. R. Karade, S. K. Bhattacharyya, M. M. Yousuf, and S. Ahalawat, “Beneficial role of nanosilica in cement based materials – A review,” *Construction and Building Materials*, vol. 47, pp. 1069–1077, Oct. 2013, doi: 10.1016/j.conbuildmat.2013.05.052.
[29] A. K. Mukhopadhyay, “Next-generation nano-based concrete construction products: a review,” *Nanotechnology in civil infrastructure*, pp. 207–223, 2011.
[30] L. G. Li, J. Y. Zheng, J. Zhu, and A. K. H. Kwan, “Combined usage of micro-silica and nano-silica in concrete: SP demand, cementing efficiencies and synergistic effect,” *Construction and Building Materials*, vol. 168, pp. 622–632, Apr. 2018, doi: 10.1016/j.conbuildmat.2018.02.181.
[31] M. Jalal, A. Pouladkhan, O. F. Harandi, and D. Jafari, “Comparative study on effects of Class F fly ash, nano silica and silica fume on properties of high performance self compacting concrete,” *Construction and Building Materials*, vol. 94, no. 90, p. 104, 2015.
[32] D. De Domenico and G. Ricciardi, “Shear strength of RC beams with stirrups using an improved Eurocode 2 truss model with two variable-inclination compression struts,” *Engineering Structures*, vol. 198, p. 109359, Nov. 2019, doi: 10.1016/j.engstruct.2019.109359.
[33] L. Sadowski, M. Nikoo, and M. Nikoo, “Concrete compressive strength prediction using the imperialist competitive algorithm,” *Computers and Concrete*, vol. 22, no. 4, pp. 355–363, 2018.
[34] S. Czarnecki, M. Shariq, M. Nikoo, and Ł. Sadowski, “An intelligent model for the prediction of the compressive strength of cementitious composites with ground granulated blast furnace slag based on ultrasonic pulse velocity measurements,” *Measurement*, vol. 172, p. 108951, Feb. 2021, doi: 10.1016/j.measurement.2020.108951.
[35] Ł. Sadowski, M. Piechówka-Mielnik, T. Widziszowski, A. Gardynik, and S. Mackiewicz, “Hybrid ultrasonic-neural prediction of the compressive strength of environmentally friendly concrete screeds with high volume of waste quartz mineral dust,” *Journal of Cleaner Production*, vol. 212, pp. 727–740, Mar. 2019, doi: 10.1016/j.jclepro.2018.12.059.
[36] C. T. G. Awodiji, D. O. Onwuka, C. Okere, and O. Ibearugbulem, “Anticipating the Compressive Strength of Hydrated Lime Cement Concrete Using Artificial Neural Network Model,” *Civil Engineering Journal*, vol. 4, no. 12, p. 3005, Dec. 2018, doi: 10.28991/cej-03091216.
[37] J. Kasperkiewicz, J. Racz, and A. Dubrawski, “HPC Strength Prediction Using Artificial Neural Network,” *Journal of Computing in Civil Engineering*, vol. 9, no. 4, pp. 279–284, Oct. 1995, doi: 10.1061/(ASCE)0887-3801(1995)9:4(279).
[38] E. Ghafari, M. Bandarabadi, H. Costa, and E. Júlio, “Design of UHPC using artificial neural networks,” in *Brittle Matrix Composites 10*, Elsevier, 2012, pp. 61–69. doi: 10.1533/9780857099891.61.
[39] M. F. Javed *et al.*, “Applications of Gene Expression Programming and Regression Techniques for Estimating Compressive Strength of Bagasse Ash based Concrete,” *Crystals*, vol. 10, no. 9, p. 737, Aug. 2020, doi: 10.3390/cryst10090737.
[40] S. A. Emamian and H. Eskandari-Naddaf, “Genetic programming based formulation for compressive and flexural strength of cement mortar containing nano and micro silica after freeze and thaw cycles,” *Construction and Building Materials*, vol. 241, p. 118027, Apr. 2020, doi: 10.1016/j.conbuildmat.2020.118027.
[41] A. Behnood and E. M. Golafshani, “Predicting the compressive strength of silica fume concrete using hybrid artificial neural network with multi-objective grey wolves,” *Journal of Cleaner Production*, vol. 202, pp. 54–64, Nov. 2018, doi: 10.1016/j.jclepro.2018.08.065.

[42] M. Hassan and K. Wille, “Experimental impact analysis on ultra-high performance concrete (UHPC) for achieving stress equilibrium (SE) and constant strain rate (CSR) in Split Hopkinson pressure bar (SHPB) using pulse shaping technique,” *Constr Build Mater*, vol. 144, pp. 747–757, Jul. 2017, doi: 10.1016/j.conbuildmat.2017.03.185.
[43] H.-O. Jang, H.-S. Lee, K. Cho, and J. Kim, “Experimental study on shear performance of plain construction joints integrated with ultra-high performance concrete (UHPC),” *Construction and Building Materials*, vol. 152, pp. 16–23, Oct. 2017, doi: 10.1016/j.conbuildmat.2017.06.156.
[44] K. Wille and C. Boisvert-Cotulio, “Material efficiency in the design of ultra-high performance concrete,” *Construction and Building Materials*, vol. 86, pp. 33–43, Jul. 2015, doi: 10.1016/j.conbuildmat.2015.03.087.
[45] K.-Q. Yu, J.-T. Yu, J.-G. Dai, Z.-D. Lu, and S. P. Shah, “Development of ultra-high performance engineered cementitious composites using polyethylene (PE) fibers,” *Construction and Building Materials*, vol. 158, pp. 217–227, 2018.
[46] F. A. Hashim, E. H. Houssein, M. S. Mabrouk, W. Al-Atabany, and S. Mirjalili, “Henry gas solubility optimization: A novel physics-based algorithm,” *Future Generation Computer Systems*, vol. 101, pp. 646–667, Dec. 2019, doi: 10.1016/j.future.2019.07.015.
[47] V. Mohebbi, A. Naderifar, R. M. Behbahani, and M. Moshfeghian, “Determination of Henry’s law constant of light hydrocarbon gases at low temperatures,” *The Journal of Chemical Thermodynamics*, vol. 51, pp. 8–11, Aug. 2012, doi: 10.1016/j.jct.2012.02.014.
[48] T. L. Brown, *Chemistry: the central science*. Pearson Education, 2009.
[49] R. Eberhart and J. Kennedy, “A new optimizer using particle swarm theory,” in *MHS’95. Proceedings of the Sixth International Symposium on Micro Machine and Human Science*, IEEE, pp. 39–43. doi: 10.1109/MHS.1995.494215.
[50] A. Maleki, “Optimal operation of a grid-connected fuel cell based combined heat and power systems using particle swarm optimisation for residential sector,” *International Journal of Ambient Energy*, vol. 42, no. 5, pp. 550–557, Apr. 2021, doi: 10.1080/01430750.2018.1562968.
[51] G. Perampalam, K. Poologanathan, S. Gunalan, J. Ye, and B. Nagaratnam, “Optimum Design of Cold-formed Steel Beams: Particle Swarm Optimisation and Numerical Analysis,” *ce/papers*, vol. 3, no. 3–4, pp. 205–210, Sep. 2019, doi: 10.1002/cepa.1159.
[52] F. Masoumi, S. Najjar-Ghabel, A. Safarzadeh, and B. Sadaghat, “Automatic calibration of the groundwater simulation model with high parameter dimensionality using sequential uncertainty fitting approach,” *Water Supply*, vol. 20, no. 8, pp. 3487–3501, Dec. 2020, doi: 10.2166/ws.2020.241.
[53] M. B. Patil, M. N. Naidu, A. Vasan, and M. R. R. Varma, “Water distribution system design using multi-objective particle swarm optimisation,” *Sādhanā*, vol. 45, no. 1, p. 21, Dec. 2020, doi: 10.1007/s12046-019-1258-y.
[54] L. Wang, *Support vector machines: theory and applications*, vol. 177. Springer Science & Business Media, 2005.
[55] V. Vapnik, *The nature of statistical learning theory*. Springer science & business media, 2013.
[56] A. Al-Fugara, M. Ahmadlou, A. R. Al-Shabeeb, S. AlAyyash, H. Al-Amoush, and R. Al-Adamat, “Spatial mapping of groundwater springs potentiality using grid search-based and genetic algorithm-based support vector regression,” *Geocarto International*, pp. 1–20, 2020.
[57] G. Pazouki, E. M. Golafshani, and A. Behnood, “Predicting the compressive strength of self-compacting concrete containing Class F fly ash using metaheuristic radial basis function neural network,” *Structural Concrete*, Feb. 2021, doi: 10.1002/suco.202000047.

APPENDIX A:

```
% PSO-SVR for UHPC Compressive Strength Prediction

% Step 1: Load and preprocess the data
data = load('uhpc_data.mat');
X = data.features; % Input features
y = data.labels; % Compressive strength labels

% Step 2: Split the data into training and testing sets
ratio = 0.8; % Training-testing data ratio
splitIdx = round(ratio * size(X, 1));
X_train = X(1:splitIdx, :);
y_train = y(1:splitIdx);
X_test = X(splitIdx+1:end, :);
y_test = y(splitIdx+1:end);

% Step 3: Define the objective function for SVR
objective = @(x)svrObjective(x, X_train, y_train);

% Step 4: Define the PSO parameters
nParticles = 50; % Number of particles
nVariables = size(X_train, 2); % Number of variables (dimensionality)
maxIterations = 100; % Maximum number of iterations

% Step 5: Initialize the PSO parameters
particlePositions = rand(nParticles, nVariables); % Initialize positions randomly
particleVelocities = zeros(nParticles, nVariables); % Initialize velocities to zero
personalBestPositions = particlePositions; % Initialize personal best positions
personalBestValues = inf(nParticles, 1); % Initialize personal best values
globalBestPosition = zeros(1, nVariables); % Initialize global best position
globalBestValue = inf; % Initialize global best value

% Step 6: Perform PSO iterations
for iteration = 1:maxIterations
    % Evaluate current positions
    particleValues = objective(particlePositions);

    % Update personal best positions and values
    updateIndices = particleValues < personalBestValues;
    personalBestPositions(updateIndices, :) = particlePositions(updateIndices, :);
    personalBestValues(updateIndices) = particleValues(updateIndices);

    % Update global best position and value
    [minValue, minIndex] = min(personalBestValues);
    if minValue < globalBestValue
        globalBestPosition = personalBestPositions(minIndex, :);
        globalBestValue = minValue;
    end

    % Update particle velocities and positions
    inertiaWeight = 0.9; % Inertia weight
    cognitiveWeight = 2; % Cognitive weight
    socialWeight = 2; % Social weight
```

```
    r1 = rand(nParticles, nVariables);
    r2 = rand(nParticles, nVariables);
    particleVelocities = inertiaWeight * particleVelocities ...
        + cognitiveWeight * r1 .* (personalBestPositions - particlePositions) ...
        + socialWeight * r2 .* (globalBestPosition - particlePositions);
    particlePositions = particlePositions + particleVelocities;

    % Perform boundary handling (if necessary)
    % e.g., particlePositions = max(min(particlePositions, upperBounds), lowerBounds);
end

% Step 7: Predict the compressive strength using the trained SVR model
predictedValues = svrPredict(X_test, globalBestPosition);

% Step 8: Evaluate the prediction performance
mse = mean((predictedValues - y_test).^2); % Mean Squared Error
rmse = sqrt(mse); % Root Mean Squared Error
mae = mean(abs)
```